Scientific Research Publishing

Agricultural Sciences, 2026, 17(9), 941-958
https://www.scirp.org/journal/as
ISSN Online: 2156-8561
ISSN Print: 2156-8553

Design and Composite Disturbance-Rejection Control of an Underactuated End Effector for Apple Harvesting

Jianan Gao

School of Agricultural Engineering, Jiangsu University, Zhenjiang, China
Email: bubbw886oc60@163.com

How to cite this paper: Gao, J.N. (2026) Design and Composite Disturbance-Rejection Control of an Underactuated End Effector for Apple Harvesting. *Agricultural Sciences*, **17**, 941-958.
https://doi.org/10.4236/as.2026.179053

Received: August 11, 2026
Accepted: September 14, 2026
Published: September 17, 2026

Abstract

To improve the harvesting adaptability and motion-control performance of apple-harvesting end effectors in complex canopy environments, an underactuated enveloping-and-cutting end effector integrating fruit capture, stem cutting, and fruit collection was developed. The device employs a cylindrical fruit passage and a pair of symmetrically arranged swinging cutter heads actuated by traction wires and torsion springs, enabling the enveloping harvesting of apples of different sizes while reducing large-amplitude twisting and pulling motions. Considering the displacement-dependent elastic load generated by the torsion springs, a dynamic model of the electric drive system was established with the motor shaft as the reference. On this basis, a composite control strategy combining load-observer-based feedforward compensation with second-order active disturbance rejection control (ADRC) was developed. The Luenberger load-torque observer estimates the equivalent torsion-spring load online and generates the corresponding feedforward compensation term, while the extended state observer (ESO) estimates residual disturbances arising from model uncertainties and external disturbances for real-time compensation. MATLAB/Simulink simulations were conducted to compare closed-loop position control, elastic-load feedforward compensation, and the proposed composite control strategy and to evaluate its performance under time-varying external load disturbances. The results showed that the proposed strategy reached the 20 mm target position with a peak displacement of approximately 20.2 - 20.3 mm and an overshoot ratio of only 1.0% - 1.5%. The steady-state position error was maintained within approximately 0.1 - 0.2 mm, representing a reduction of about 85% compared with conventional closed-loop position control. Under imposed time-varying load torque disturbances, the maximum position deviation was approximately 0.4 mm, and the tracking error recovered to within ±0.05 mm in approximately 0.7 s. These results indicate that the proposed composite control strategy can effectively improve positioning accuracy, transient response, and disturbance-rejection performance under time-varying elastic loads and abrupt external disturbances.

Keywords

Apple Harvesting Robot, End Effector, Feedforward Compensation, Disturbance Rejection

1. Introduction

Apple ranks among the most important fresh-market fruits and economically valuable crops worldwide. China has long been a leader in both apple cultivation area and total production [1]. The large-scale transition of the apple industry increasingly exposes its heavy reliance on manual labor. Although fertilization and pesticide application have been mechanized, apple harvesting remains predominantly manual because fruits are spatially dispersed, susceptible to mechanical damage, and harvested within a short window. Apple harvesting accounts for approximately 30% - 40% of the total labor input in apple production, raising production costs and substantially constraining the industry's sustainable development [2] [3]. Therefore, developing robotic apple-harvesting systems has emerged as a promising approach to reducing production costs and improving operational efficiency in orchards [4].

In apple-harvesting robots, the end effector is a critical component for automated fruit harvesting. Responsible for executing specific harvesting operations, the end effector is a major focus of current research and optimization [5]. The end effector directly contacts the fruit and performs grasping and detachment, so its performance strongly influences the overall harvesting process. Current research focuses on damage-free harvesting and stable grasping to minimize fruit injury and enhance reliability. Therefore, optimizing the end effector's operational performance is an important research direction for improving apple-harvesting efficiency while preserving fruit quality [6]-[8].

Apple-harvesting end effectors are generally classified into three categories by harvesting mechanism: cutting, suction, and gripping [9] [10]. Cutting-type end effectors typically stabilize the fruit with a positioning mechanism and sever the stem using a rotating blade or scissor mechanism. Although cutting-type end effectors offer relatively high harvesting speeds, their operation is readily affected by interference from branches and leaves within the canopy. Therefore, their practical application requires highly accurate fruit detection and localization.

Suction-type end effectors primarily use negative-pressure suction cups to capture fruits, then detach them by twisting or pulling [11]. With limited rigid contact with the fruit surface, these end effectors adapt to fruits of different sizes while maintaining relatively simple structures. To further reduce harvesting damage, some designs incorporate flexible suction cups and multi-stage cushioning mechanisms. Such designs reduce collisions during fruit suction and transportation, thereby improving harvesting safety and reliability. Baeten *et al.* [12] developed a negative-pressure suction end effector with a funnel-shaped suction inlet. Once the camera detected the target apple within harvesting range, negative pressure drew the fruit into the end effector. Drawing on apple characteristics and octopus predatory behavior, Wang *et al.* [13] developed a novel biomimetic apple-harvesting gripper using negative-pressure suction. During harvesting, the suction cup deformed concavely under negative pressure and closely conformed to the apple surface, providing stable adhesion.

However, under actual orchard canopy conditions, suction performance may be affected by fruit orientation, surface curvature, occlusion by branches and leaves, and the degree of conformity between the suction cup and the fruit surface. Moreover, secondary damage to fruits may also occur during suction, transportation and release. Therefore, further improvements are required in the grasping stability and low-damage transport capability of suction-type end effectors.

Gripping-type end effectors primarily employ multi-finger grippers, underactuated fingers, or tendon-driven mechanisms to grasp and envelop the fruit, detaching it via rotational or pulling motions generated by the robotic arm or the end effector itself. Compared with suction-type end effectors, gripping-type ones generally provide greater load-bearing capacity and higher grasping stability. Avigad *et al.* [14] developed a three-finger underactuated end effector that mimics manual apple picking. However, its abrupt harvesting motion risked substantial shaking of surrounding branches and unintended detachment of nearby fruits. Silwal *et al.* [15] developed a tendon-driven three-finger end effector, where an actuator regulated tendon tension to control fruit grasping and release. However, excessive gripping force or relative motion between fingers and fruit can readily cause skin abrasion and flesh bruising. To balance grasping stability with fruit protection, flexible materials, biomimetic fingers, and compliant mechanisms have been incorporated into end-effector designs. These approaches reduce localized stress during gripping by increasing contact area, promoting uniform contact force distribution, and adapting to fruits of different diameters [16]. Nevertheless, the structural stiffness, load-bearing capacity, and actuation speed of these designs are generally limited by the properties of the flexible materials and actuation methods employed.

To further reduce fruit damage and improve harvesting accuracy, researchers have investigated control methods for end effectors. Wang *et al.* [17] incorporated fuzzy control into a hybrid force/position control system, providing online compensation for errors caused by model uncertainties and external disturbances and effectively improving force-and position-tracking performance. Zhang *et al.* [18] developed a hybrid force/position control method based on a fuzzy PID controller. By coordinating the velocity loop with the fuzzy PID controller, the method enhanced the robotic grinding system's adaptability to external disturbances and parameter variations, offering a useful reference for disturbance-rejection control strategies in harvesting robots under complex load conditions.

To address the aforementioned limitations, this study focused on two aspects: developing an underactuated end effector with swinging blades for stem severing to enable enveloping harvesting of different-sized apples; and, based on the end effector's motion and operational characteristics, developing an actuator control method combining feedforward compensation with second-order active disturbance rejection control and evaluating its effectiveness and feasibility through simulations.

2. Materials and Methods

2.1. Design of an Apple-Harvesting End Effector

To achieve damage-free harvesting in complex apple canopy environments, this study developed an enveloping-and-cutting end effector that integrates fruit capture, stem cutting, and fruit collection, as shown in Figure 1. The end effector uses a cylindrical enclosure as a fruit passage and primarily consists of a collection cylinder, a semicircular swinging cutter head, replaceable blades, a torsion spring, a traction wire, an electric actuator, and mounting connectors. These components are axially arranged within the end effector, yielding a compact overall configuration. Its relatively smooth external contour reduces the risk of collision and scraping against branches and adjacent fruits during canopy entry. A pair of semicircular swinging cutter heads is symmetrically mounted at the distal opening of the end effector, with replaceable cutting blades at their distal ends, torsion springs around the pivot shafts, and traction wires connecting the cutter heads to the actuator.

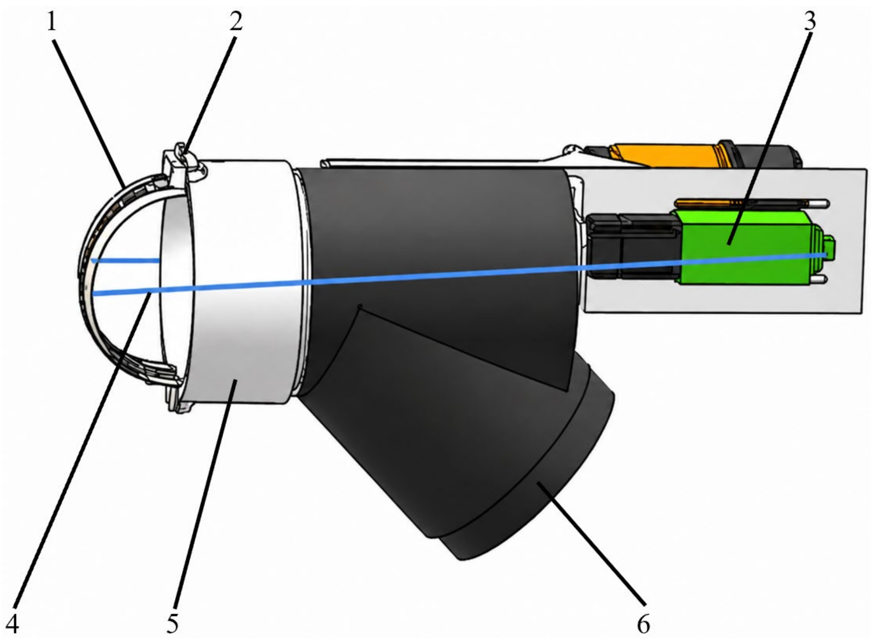

Note: 1. Semicircular swinging cutter head, 2. Torsion spring, 3. Electric actuator, 4. Traction wire, 5. Collection cylinder, 6. Collection channel.

Figure 1. Structure of the apple-harvesting end effector.

The designed end effector is capable of accommodating apples with diameters ranging from 65 mm to 90 mm. The two semicircular swinging cutter heads provide an angular motion range of 90˚ (from the fully opened position to the closed cutting position), enabling the mechanism to adapt to variations in fruit size and stem position during harvesting. The torsion springs installed at the cutter-head pivots provide the restoring torque required for cutter-head closure, with a torsional stiffness of 0.3266 N·m/rad and an initial preload angle of 30˚.

The harvesting cycle of the enveloping-and-cutting end effector consists of four sequential stages: cutter-head opening, fruit capture, stem cutting, and mechanism resetting. Before harvesting, the actuator retracts, pulling the two swinging cutter heads open via the traction wires and overcoming the restoring torque of the torsion springs, thereby placing the end effector in a fruit-capture-ready state. As the cutter heads rotate open, the torsion springs gradually store elastic potential energy. Once fully opened, the actuator holds the cutter heads open. The robotic arm then guides the end effector toward the target apple and adjusts the distal opening's position and orientation relative to the fruit, allowing the apple to enter the enveloping space.

After the robotic arm completes positioning, the actuator rapidly extends as commanded, releasing the traction wires. The torsion springs release the stored elastic potential energy, driving the two swinging cutter heads to close synchronously. During closure, the cutter heads envelop and constrain the fruit, and the distal blades simultaneously sever the stem, coordinating fruit capture with stem separation. The detached fruit then passes through the collection cylinder into the downstream conveying channel. The actuator then retracts, pulling the cutter heads back to the preset open position and resetting the mechanism for the next cycle. This method eliminates the need for additional large-amplitude twisting or pulling motions by the robotic arm and a separate fruit-release operation, simplifying the overall harvesting process.

2.2. Dynamic Model of the End-Effector Actuator

During the cutting and resetting operations, the actuator is subjected to complex loads broadly classified as internal system loads and external environmental disturbances. Internal loads mainly arise from the inertia of moving components, transmission friction, and the torsion-spring restoring force, which varies with the cutter-head opening angle and thus constitutes a displacement-dependent time-varying load. External disturbances, primarily from fruit contact, branch and leaf collisions, and mechanical clearances, exhibit substantial randomness and uncertainty. Given these characteristics, only the torsion-spring elasticity is explicitly retained in the system model to simplify controller design while preserving dominant dynamics; small elastic deformations of other transmission components are neglected. System friction, canopy collision disturbances, and unmodeled dynamics are collectively lumped into the total disturbance, providing a unified representation of uncertainties and disturbances for subsequent controller design.

The end-effector actuator uses a permanent magnet synchronous motor (PMSM) as the power source; rotational motion is converted to linear motion via a lead-screw mechanism, and the resulting linear displacement is amplified fourfold by the actuator's internal transmission. To facilitate controller design and highlight the influence of the torsion-spring elastic load, the system is simplified by neglecting the inertia of moving components (including the lead-screw mechanism, traction wires, and swinging cutter heads) and frictional damping in the transmission. Accordingly, only the motor rotor inertia and the torsion-spring elastic load are explicitly considered. A dynamic model is then established with the motor shaft as the reference, where the elastic load from the torsion springs is equivalently converted into a load torque acting on the motor shaft.

The dynamic equation on the motor rotational side is given by:

$$J_m \ddot{\theta} = T_m - T_L \tag{1}$$

where J_m denotes the equivalent rotational inertia of the motor rotor; θ denotes the motor angular position; T_m denotes the electromagnetic torque generated by the motor; and T_L denotes the equivalent load torque generated by the torsion-spring elastic force and referred to the motor shaft.

The motor output motion is converted into linear motion through the lead-screw mechanism. Let p denote the lead of the screw. The relationship between the displacement of the actuator output end and the motor angular position can then be expressed as:

$$x = \frac{2p}{\pi}\theta \tag{2}$$

The traction wire is connected to the end of the torsion-spring swing arm. Let R denote the distance from the connection point to the center of the torsion spring. As the swing arm rotates, the connection point moves along a circular path, and the corresponding change in arc length can be expressed as:

$$x = R\varphi \tag{3}$$

where φ denotes the rotation angle of the torsion-spring swing arm.

Combining Equation (2) and Equation (3) yields:

$$\varphi = \frac{x}{R} = \frac{2p}{\pi R}\theta \tag{4}$$

The elastic torque generated by the torsion spring can be expressed as:

$$M_s = K_s\left(\varphi - \varphi_0\right) \tag{5}$$

where K_s denotes the torsional stiffness of the torsion spring, and φ_0 denotes the initial preload angle of the torsion spring.

According to the principle of virtual work, the torque exerted by the torsion spring and the equivalent load torque referred to the motor shaft satisfy the following relationship:

$$T_L d\theta = M_s d\varphi \tag{6}$$

Therefore,

$$T_L = M_s \frac{d\varphi}{d\theta} \tag{7}$$

From Equation (4), it follows that:

$$\frac{d\varphi}{d\theta} = \frac{2p}{\pi R} \tag{8}$$

Substituting Equation (5) and (8) into Equation (7) yields:

$$T_L = K_s \left(\varphi - \varphi_0\right) \frac{2p}{\pi R} \tag{9}$$

Further combining Equation (4) and rearranging yields the equivalent load torque referred to the motor shaft as:

$$T_L = K_s \left(\frac{2p}{\pi R}\right)^2 \theta - K_s \varphi_0 \frac{2p}{\pi R} \tag{10}$$

Substituting Equation (10) into the motor dynamic equation, Equation (1), yields the dynamic model of the end-effector drive system considering the torsion-spring elastic load:

$$J_m \ddot{\theta} + K_s \left(\frac{2p}{\pi R}\right)^2 \theta = T_m + K_s \varphi_0 \frac{2p}{\pi R}. \tag{11}$$

Thus, the electromechanical dynamic model of the enveloping-and-cutting end effector is established. In this model, $J_m \ddot{\theta}$ represents the inertial effect of the motor rotor, while the second term represents the torsion-spring elastic load referred to the actuator output end. The terms on the right-hand side represent the motor output torque and the equivalent bias torque generated by the torsion-spring preload, respectively. The model characterizes the dynamic load variation associated with torsion-spring deformation during end-effector operation and provides a theoretical basis for the subsequent design of the control system.

2.3. Structure of the Composite Control Strategy

Based on the end-effector dynamic model, this study develops a composite control strategy combining load-observer-based feedforward compensation with second-order active disturbance rejection control (ADRC). The elastic-load feedforward compensation actively counteracts the equivalent load torque generated by the torsion springs, reducing the response lag of feedback control that acts only after tracking errors arise. Meanwhile, the second-order ADRC employs an ESO to estimate internal parameter variations and external disturbances online and compensate for them in real time, enhancing the system's disturbance-rejection capability.

The overall structure of the proposed control strategy is shown in **Figure 2**. The system takes the desired position command as the input. The load-torque observer uses motor feedback information to estimate the equivalent torsion-spring load online and converts the estimated load into a feedforward compensation term.

Meanwhile, the ESO estimates and compensates for residual disturbances caused by model uncertainties and external load variations.

The total control input of the system can be expressed as:

$$i_q^* = i_{q,fb}^* + i_{q,ff}^* \tag{12}$$

where u_{ADRC} denotes the control output of the ADRC, and u_{ff} denotes the elastic-load feedforward compensation term.

The motor angular position is converted into the actuator linear displacement according to Equation (2), and the corresponding position and velocity signals are fed back to the outer motion-control loop.

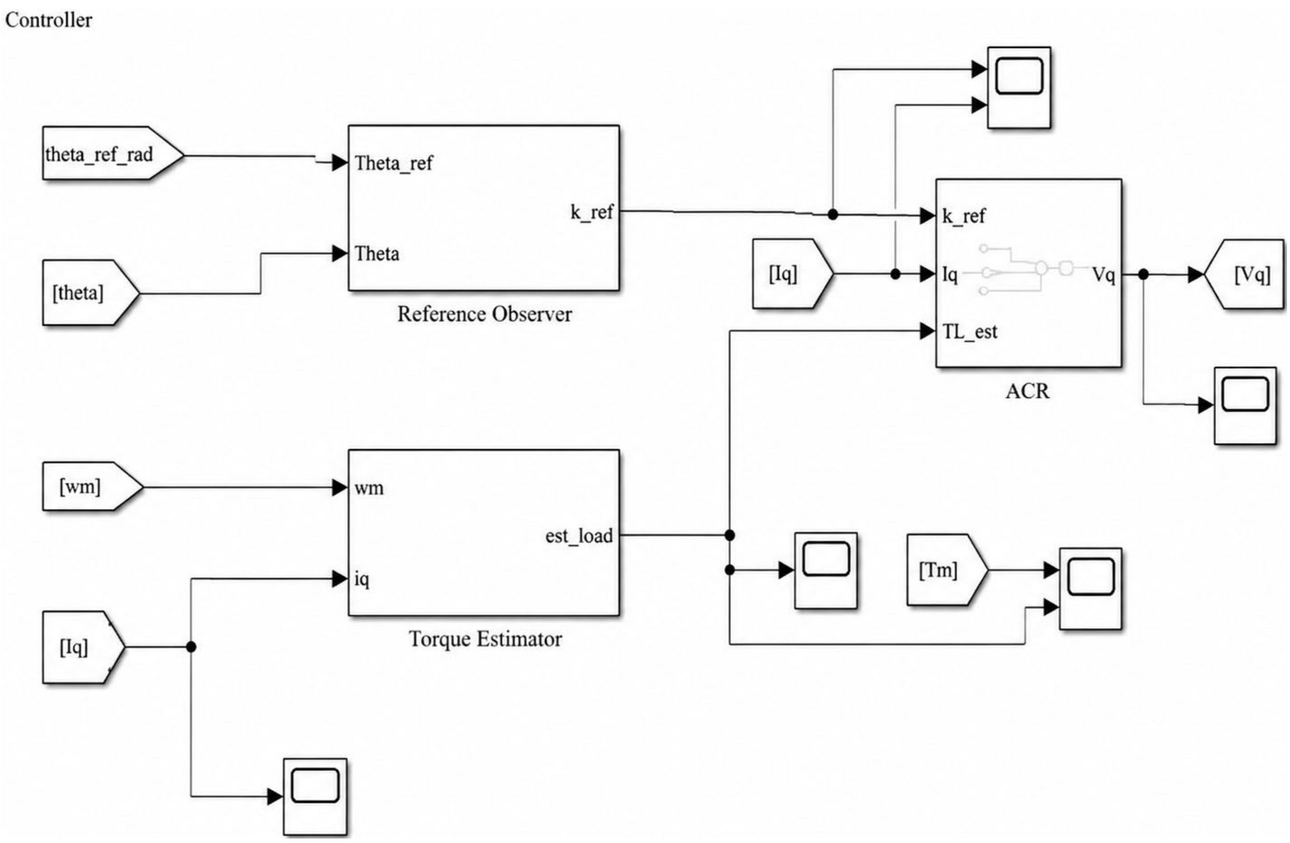

Figure 2. Control strategy framework.

2.4. Feedforward Compensation Control Law

After being referred to the motor shaft through the transmission mechanism, the torsion-spring elastic load is represented as a load torque T_L that varies with the motion state of the system. Since this load torque is difficult to measure directly, a load-torque observer is constructed based on the PMSM dynamic model established in the previous section to achieve online estimation of T_L. Considering that the load variation can be regarded as a slowly varying process within a short control period, it is assumed that:

$$\dot{T}_L \approx 0 \tag{13}$$

The motor mechanical angular velocity and load torque are then selected as the state variables:

$$x = \begin{bmatrix} \omega_m & T_L \end{bmatrix}^T . \tag{14}$$

Based on the model established in the previous section, a Luenberger observer can be constructed as:

$$\begin{cases} \dot{\hat{\omega}}_m = -\dfrac{B}{J}\hat{\omega}_m - \dfrac{1}{J}\hat{T}_L + \dfrac{K_t}{J}i_q + l_1\left(\omega_m - \hat{\omega}_m\right) \\ \dot{\hat{T}}_L = l_2\left(\omega_m - \hat{\omega}_m\right) \end{cases} \tag{15}$$

where $\hat{\omega}_m$ and $\hat{T}_L$ denote the estimated mechanical angular velocity and load torque, respectively; and l_1 and l_2 are the observer gains. By appropriately assigning the observer poles such that the eigenvalues of the observation error system are located in the left half of the complex plane, the estimated load torque can be guaranteed to converge asymptotically to its actual value. This method indirectly reconstructs the load torque using the motion-state information obtained from the encoder and the motor control input, without requiring additional force or torque sensors.

After obtaining the estimated load torque $\hat{T}_L$, it is converted into a feedforward compensation current according to the relationship between the electromagnetic torque and the q-axis current:

$$i_{q,ff}^* = \frac{\hat{T}_L}{K_t} \tag{16}$$

Accordingly, the final q-axis current command can be expressed as:

$$i_q^* = i_{q,fb}^* + \frac{\hat{T}_L}{K_t} \tag{17}$$

where $i_{q,fb}^*$ denotes the q-axis current reference generated by the position/velocity disturbance-rejection controller. The feedforward compensation current $i_{q,ff}^*$ is added directly to the q-axis current reference before entering the inner current loop. The resulting command i_q^* is then tracked by the motor-current controller.

2.5. Second-Order Active Disturbance Rejection Control Model

Although elastic-load feedforward control compensates for the predictable torsion-spring load, the harvesting mechanism exhibits significant nonlinearities and parameter uncertainties, making satisfactory control using the load model alone difficult. Nonlinear friction variations, transmission clearances, parameter deviations, and load-observation errors can cause discrepancies between the actual load and its model-based estimate, resulting in residual feedforward-compensation errors.

Meanwhile, fruit harvesting is subject to external disturbances that are difficult to characterize accurately with mathematical models. Abrupt, uncertain transient impacts from canopy collisions and stem cutting can deviate system states from the desired trajectory, further degrading dynamic control performance. To further enhance disturbance rejection, a control mechanism capable of online disturbance estimation and real-time compensation is required to improve the motion-control accuracy and stability of the harvesting mechanism under complex operating conditions.

To this end, a second-order active disturbance rejection control (ADRC) method is adopted, in which the internal uncertainties and external disturbances of the system are collectively treated as the total disturbance and are estimated and compensated online using ESO.

The motor position control system can be simplified as:

$$\ddot{\theta} = b_0 u + d\left(t\right) \tag{18}$$

where θ denotes the motor angular position; u denotes the equivalent feedback control input generated by the position/velocity ADRC and subsequently mapped to the q-axis feedback current reference $i_{q,fb}^{*}$; b_0 denotes the nominal input gain of the outer motion-control model; and $d\left(t\right)$ denotes the lumped disturbance acting on the position/velocity dynamics.

The extended state variables are defined as:

$$x_1 = \theta, x_2 = \dot{\theta}, x_3 = d\left(t\right) \tag{19}$$

The state-space equations of the system can then be expressed as:

$$\begin{cases} \dot{x}_1 = x_2 \\ \dot{x}_2 = x_3 + b_0 u \\ \dot{x}_3 = \dot{d}\left(t\right) \\ y = x_1 \end{cases} \tag{20}$$

where x_1 and x_2 denote the position and velocity states, respectively; x_3 denotes the extended state, representing the total disturbance of the system; and y denotes the position output.

Accordingly, the ESO is constructed as:

$$\begin{cases} e_o = z_1 - y \\ \dot{z}_1 = z_2 - \beta_1 e_o \\ \dot{z}_2 = z_3 - \beta_2 e_o + b_0 u \\ \dot{z}_3 = -\beta_3 e_o \end{cases} \tag{21}$$

where e_o denotes the observation error; z_1, z_2, and z_3 denote the estimated position, velocity, and total disturbance, respectively; and β_1, β_2, and β_3 are the observer gains.

The feedback control law is constructed based on the position and velocity errors, and the estimated disturbance is incorporated for compensation, yielding the final control input as:

$$u_{ADRC} = \frac{k_p\left(\theta_r - z_1\right) + k_d\left(\dot{\theta}_r - z_2\right) - z_3}{b_0} \tag{22}$$

where θ_r and $\dot{\theta}_r$ denote the reference position and reference velocity, respectively; k_p and k_d denote the position and velocity feedback gains, respectively; and z_3 denotes the total disturbance estimated by the ESO.

The ADRC output u_{ADRC} is used to generate the feedback q-axis current reference $i^*_{q,fb}$ in the outer position/velocity control loop. This feedback current reference is subsequently combined with the torsion-spring feedforward current $i^*_{q,ff}$ according to Equation (17). The resulting i^*_q is applied as the reference input to the inner q-axis current loop.

When z_3 can accurately track the total disturbance $d(t)$, the ADRC can compensate in real time for disturbances such as variations in friction, transmission impacts, and random canopy collisions, thereby reducing the actuator position error and improving the tracking accuracy and operational stability of the end effector during harvesting.

3. Simulation Analysis

To evaluate the control performance of the proposed composite control strategy for the end-effector drive system, a system simulation model was established in MATLAB/Simulink based on the aforementioned dynamic model and control structure. Considering the load variations and external disturbances that may occur during actual harvesting operations, the system performance was analyzed in terms of position-tracking response, load-tracking variations, and positioning errors.

In the simulation study, a predefined bounded time-varying load torque disturbance is introduced as a representative external disturbance input to evaluate the disturbance-rejection capability of the controller. This disturbance is used for robustness assessment and does not represent the exact force history of a specific fruit-branch collision event.

3.1. Simulation Conditions and Reference Trajectory

According to the actual operating sequence of the end effector, a piecewise position reference was specified. For t < 0.5 s, the actuator remained at its initial position of 0. For 0.5 s < t < 1.2 s, the reference position was gradually increased from 0 to 0.02 m, thereby simulating the process in which the actuator pulls the swinging cutter head to open the end effector. For t > 1.2 s, the reference position was maintained at 0.02 m, representing the condition in which the cutter head remains open during fruit capture. The simulation time step was set to 1×10^{-4} s, and the total simulation duration was 5 s.

In the simulation, the motor is implemented using the built-in standard permanent magnet synchronous motor (PMSM) model in MATLAB/Simulink. The mechanical parameters are set as follows: $J_m = 3.0555\times10^{-4}\,\mathrm{kg\cdot m^2}$, and viscous friction coefficient $B_m = 3.339\times10^{-3}\,\mathrm{N\cdot m\cdot s/rad}$. The mechanical load is applied in the form of a torque input. The inverter switching frequency is set to $f_s = 5\mathrm{kHz}$, corresponding to a sampling period of $T_s = 2\times10^{-4}\,\mathrm{s}$. The controller simulation parameters are summarized in Table 1.

Table 1. Simulation parameters.

Controller	Parameter	Value
Luenberger Observer	l_1	89.0722
	l_2	−1.52775
ESO	β_1	100
	β_2	3333
	β_3	31250
	ω_o	33.3
ADRC	b_0	0.00125
	K_p	2000
	K_d	5

3.2. Simulation Scenario 1

To evaluate the proposed composite control strategy and further clarify the specific contribution of each control component, three comparative schemes were established under identical system parameters, initial conditions, control periods, reference trajectories, and disturbance conditions. Scheme 1 employed a conventional PI-based closed-loop position controller as the baseline control scheme, where the proportional gain and integral gain were set to $\hat{K}_p = 5.5$ and $\hat{K}_i = 1.8$, respectively. No elastic-load feedforward compensation or disturbance observer was included in this baseline controller. Scheme 2 added elastic-load feedforward compensation to the PI-based closed-loop position controller to evaluate the improvement obtained from compensating the predictable torsion-spring load. Scheme 3 further incorporated ESO-based disturbance compensation, constituting the proposed composite control strategy. By progressively adding control components while all other conditions remained unchanged, the responses of the three schemes were directly compared to evaluate the individual contributions of elastic-load feedforward and ESO-based compensation to system dynamic performance and disturbance rejection.

3.3. Simulation Scenario 2

To evaluate the disturbance-rejection capability of the proposed composite control strategy under canopy collision disturbances, a predefined time-varying load torque disturbance was introduced during the interval of 2.5 s < t < 3.5 s, with all other conditions identical to Simulation Scenario 1. The disturbance signal was directly applied to the mechanical load input of the PMSM model. This disturbance was designed as a representative bounded transient load variation for controller robustness evaluation rather than a quantitative reproduction of actual orchard contact forces.

Before disturbance occurrence, the load torque was maintained at approximately 18 N·m. After 2.5 s, the load torque increased to approximately 22 N·m, followed by a decrease to approximately 10 N·m, and finally recovered to the initial value. The disturbance profile was implemented through the load torque input of the PMSM mechanical model.

4. Results and Discussion

4.1. Position-Tracking Performance

The actuator displacement responses under different control strategies are shown in Figure 3. The reference displacement begins to increase at 0.5 s and reaches the target value of 20 mm at approximately 1.1 - 1.2 s, corresponding to a command-transition duration of about 0.6 - 0.7 s. Under closed-loop position control alone, the system generally follows the reference trajectory during the rising stage; however, noticeable overshoot and oscillations occur during the command transition, followed by a persistent positive position error during the position-holding stage. Based on the curve in Figure 3, the displacement at 5 s is approximately 21.3 - 21.5 mm, corresponding to a position error of about 1.3 - 1.5 mm relative to the 20 mm target and a relative error of approximately 6.5% - 7.5%. This behavior can be attributed primarily to the fact that the torsion-spring restoring force, mechanical friction, and external loads are compensated only indirectly through position-error feedback, limiting the controller's ability to promptly counteract the displacement-dependent elastic load. These results indicate that closed-loop position control alone exhibits relatively slow convergence and a pronounced residual error during the position-holding stage, making it difficult to meet the high-precision positioning requirements of the end effector.

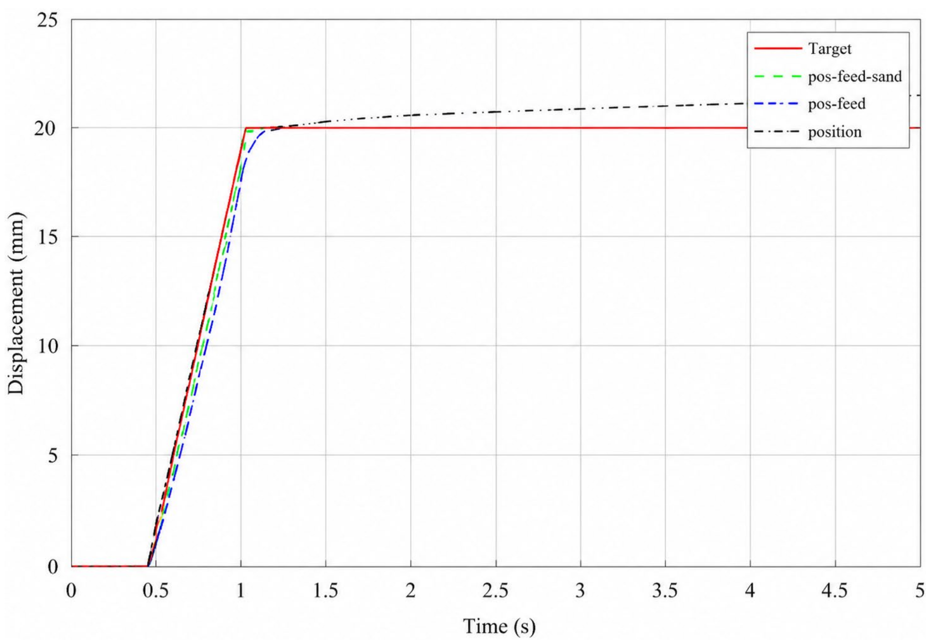

Figure 3. Comparison of position-tracking responses.

Compared with closed-loop position control alone, incorporating elastic-load feedforward compensation significantly improves the system's dynamic response. By estimating and compensating for the torsion-spring restoring force in advance, the controller reduces reliance on position-error feedback for elastic-load compensation, accelerating the system response and substantially reducing overshoot and oscillations. However, feedforward compensation effectiveness strongly depends on the nominal torsion-spring load model accuracy and may be degraded by parameter deviations, nonlinear friction, and external disturbances. Therefore, although elastic-load feedforward compensation effectively mitigates the predictable elastic load effect on the position response, residual tracking errors may still arise from model mismatch and unknown disturbances.

Further incorporating an ESO into the elastic-load feedforward compensation scheme enables online estimation and compensation of load variations and external disturbances not captured by the nominal model, further improving position response smoothness. Under the proposed composite control strategy, the displacement response reaches the vicinity of the 20 mm target at approximately 1.1 - 1.2 s, with a peak displacement of about 20.2 - 20.3 mm. The maximum overshoot is approximately 0.2 - 0.3 mm, corresponding to an overshoot ratio of 1.0% - 1.5%. At steady state, the position error remains within approximately 0.1 - 0.2 mm, with no noticeable sustained oscillations. Compared with the terminal position error of 1.3 - 1.5 mm under closed-loop position control alone, the proposed strategy reduces the steady-state position error by approximately 85%, demonstrating effective compensation of residual loads and unknown disturbances. These results indicate that elastic-load feedforward compensation primarily counteracts the predictable torsion-spring load, whereas the ESO further suppresses model mismatch and external disturbances. Their coordinated action effectively improves position-tracking accuracy, transient response, and disturbance rejection.

4.2. Nominal Model-Consistency Verification of the Load Observer

Under the nominal simulation condition, the reference load torque was generated using the same torsion-spring model and nominal parameters as those adopted in the plant model. Therefore, the comparison shown in **Figure 4** is intended as a model-consistency verification of the load observer rather than an independent robustness test. The model-generated load torque was compared with the observer-estimated load torque to verify whether the observer could reconstruct the nominal displacement-dependent elastic load used for feedforward compensation.

As the actuator extension increases, the elastic load generated by the torsion spring increases progressively. During actuator motion, the model-generated load torque varies approximately linearly with actuator displacement, consistent with the relationship between torsion-spring torque and angular deflection. The observer-estimated load exhibits a slight tracking lag during the load-increasing stage but rapidly converges toward the model-generated value. Once the actuator reaches the target position and enters the position-holding stage, the estimated load remains close to the nominal load value without noticeable sustained oscillations or appreciable steady-state estimation error. These results confirm the consistency between the nominal load model and the implemented load observer. Parameter mismatch was not explicitly considered in the present simulation; therefore, the robustness of the load observer against variations in torsional stiffness, spring preload, and other mechanical parameters remains to be further evaluated.

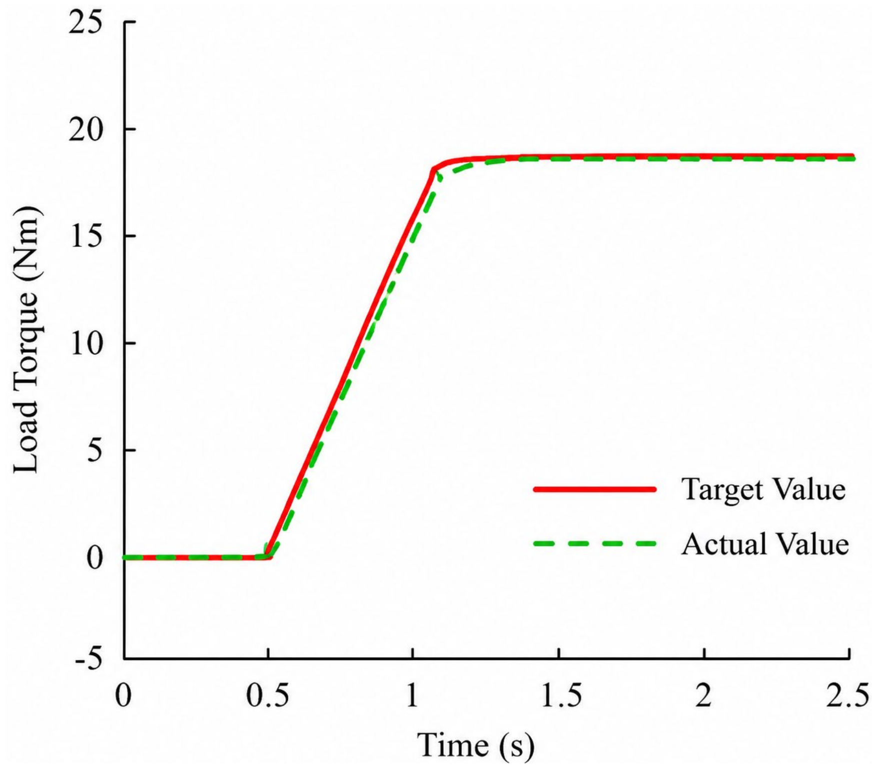

Figure 4. Nominal model-consistency verification of the load observer.

4.3. Disturbance Rejection Performance

The applied disturbance load and its estimated value are shown in **Figure 5**. After an external load change, the ESO rapidly captures and responds to the resulting disturbance variation. The estimated disturbance generally matches the actual disturbance, providing an effective basis for compensation and enabling rapid recovery to the desired operating state. Although a brief estimation lag occurs immediately after the abrupt change, the estimation error converges rapidly without sustained divergence or noticeable oscillations. These results indicate that the ESO exhibits satisfactory dynamic estimation performance and effectively tracks the applied external load torque variation. Combined with real-time compensation, this capability helps limit disturbance-induced deviations and improves the system's disturbance-rejection performance.

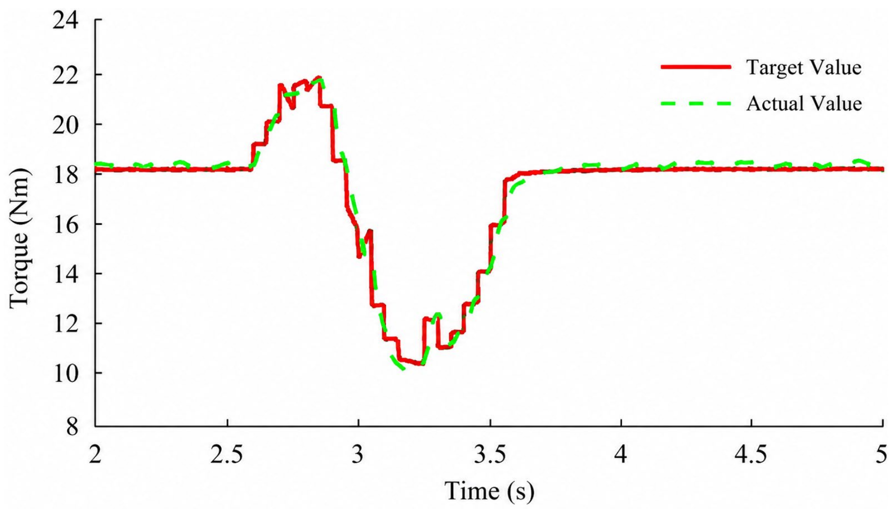

Figure 5. Load torque disturbance and ESO estimation.

4.4. Error Analysis

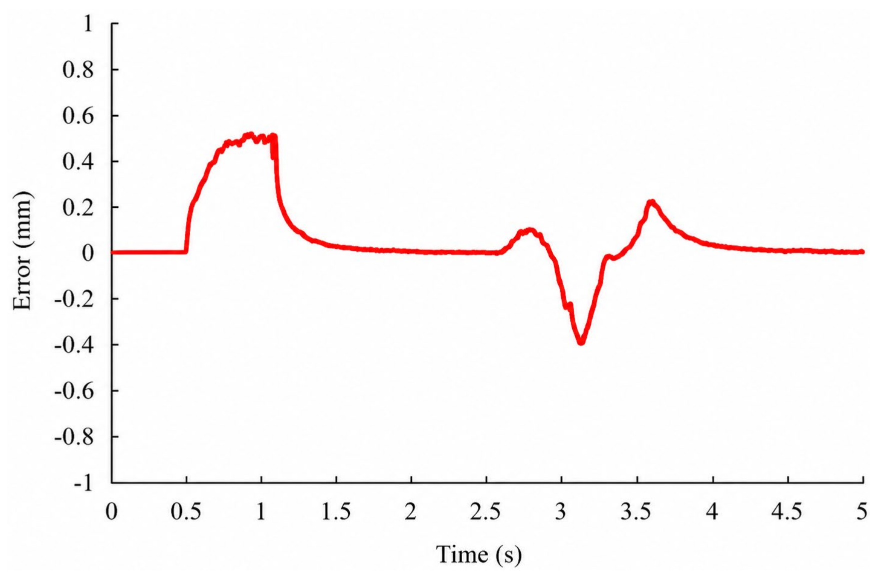

Figure 6. Position tracking error.

The position-tracking error under the proposed composite control strategy is shown in Figure 6. During startup and the gradual increase of the elastic load, the position error increases transiently with the reference position but rapidly decays after reaching the target position without sustained oscillations. The absolute position error remains within 0.6 mm overall and gradually approaches zero at steady state. Under the external disturbance, a transient negative deviation of approximately 0.4 mm occurs; upon disturbance removal, a small positive corrective deviation appears, and the error recovers to within ±0.05 mm in approximately 0.7 s. These results indicate that elastic-load feedforward compensation effectively counteracts the displacement-dependent torsion-spring load, while the ESO estimates residual disturbances from model mismatch and external disturbances for real-time compensation. Through their coordinated action, no noticeable error accumulation or sustained oscillations occur under time-varying loads or abrupt external disturbances, enabling high position-tracking accuracy, satisfactory steady-state performance, and strong disturbance-rejection capability.

5. Conclusions

In this study, an underactuated enveloping-and-cutting end effector integrating fruit capture, stem cutting, and fruit collection was developed. Through the coordinated action of the traction wire and torsion springs, the symmetrically arranged swinging cutter heads enable enveloping harvesting of apples of different sizes while simultaneously severing the fruit stems. This design reduces the need for additional twisting, pulling, and fruit-release motions by the robotic arm, thereby simplifying the overall harvesting process of the end effector.

A composite control strategy combining feedforward compensation with second-order active disturbance rejection control (ADRC) was proposed. Through the coordinated action of feedforward compensation and second-order ADRC, accurate positioning and stable position holding of the end effector during harvesting were achieved. The simulation results showed that the proposed strategy achieved an average steady-state position error of 0.15 mm and a disturbance recovery time of 0.7 s, demonstrating satisfactory positioning accuracy and disturbance rejection performance.

Author Contributions

Jianan Gao: Conceptualization, methodology, writing—original draft preparation, writing—review and editing.

Conflicts of Interest

The author declares no conflicts of interest regarding the publication of this paper.

References

[1] Chen, J. (2025) Study on Genetic Evolutionary (Domestication) Relationships in Malus. Master's Thesis, Northwest A&F University. (In Chinese)

[2] Miao, Y. and Zheng, J. (2020) Optimization Design of Compliant Constant-Force Mechanism for Apple Picking Actuator. *Computers and Electronics in Agriculture*, **170**, Article ID: 105232. https://doi.org/10.1016/j.compag.2020.105232

[3] Tang, Z., He, Y., Tang, Z., Liu, Z. and Liu, X. (2025) Research Status and Development Trends of Apple Picking Machinery. *Xinjiang Agricultural Mechanization*, No. 6, 42-47. (In Chinese)

[4] Jia, W., Tian, Y., Luo, R., Zhang, Z., Lian, J. and Zheng, Y. (2020) Detection and Segmentation of Overlapped Fruits Based on Optimized Mask R-CNN Application in Apple Harvesting Robot. *Computers and Electronics in Agriculture*, **172**, Article ID: 105380. https://doi.org/10.1016/j.compag.2020.105380

[5] Graham, S.S., Zong, W., Feng, J. and Tang, S. (2018) Design and Testing of a Kiwifruit Harvester End-Effector. *Transactions of the ASABE*, **61**, 45-51.

https://doi.org/10.13031/trans.12361

[6] Bac, C.W., Hemming, J., van Tuijl, B.A.J., Barth, R., Wais, E. and van Henten, E.J. (2017) Performance Evaluation of a Harvesting Robot for Sweet Pepper. *Journal of Field Robotics*, **34**, 1123-1139. https://doi.org/10.1002/rob.21709

[7] Kondo, N., Yamamoto, K., Shimizu, H., Yata, K., Kurita, M., Shiigi, T., *et al.* (2009) A Machine Vision System for Tomato Cluster Harvesting Robot. *Engineering in Agriculture, Environment and Food*, **2**, 60-65. https://doi.org/10.1016/s1881-8366(09)80017-7

[8] Han, C., Lv, J., Dong, C., Li, J., Luo, Y., Wu, W., *et al.* (2024) Classification, Advanced Technologies, and Typical Applications of End-Effector for Fruit and Vegetable Picking Robots. *Agriculture*, **14**, Article 1310. https://doi.org/10.3390/agriculture14081310

[9] Zhang, K., Lammers, K., Chu, P., Li, Z. and Lu, R. (2021) System Design and Control of an Apple Harvesting Robot. *Mechatronics*, **79**, Article ID: 102644. https://doi.org/10.1016/j.mechatronics.2021.102644

[10] Han, S.K., Zhao, Z.K., Zhang, H., Zhou, Y. and Wang, Z.Y. (2019) Design and Simulation Analysis of the End Effector of Circular Fruit Picking Robot. *Journal of Machine Design*, **36**, 82-85. (In Chinese) https://doi.org/10.13841/j.cnki.jxsj.2019.s2.020

[11] Hu, G., Chen, C., Chen, J., Sun, L., Sugirbay, A., Chen, Y., *et al.* (2022) Simplified 4-DOF Manipulator for Rapid Robotic Apple Harvesting. *Computers and Electronics in Agriculture*, **199**, Article ID: 107177. https://doi.org/10.1016/j.compag.2022.107177

[12] Baeten, J., Donné, K., Boedrij, S., Beckers, W. and Claesen, E. (2008) Autonomous Fruit Picking Machine: A Robotic Apple Harvester. In: Laugier, C. and Siegwart, R., Eds., *Field and Service Robotics*, Springer, 531-539. https://doi.org/10.1007/978-3-540-75404-6_51

[13] Wang, M., Yan, B., Zhang, S., Fan, P., Zeng, P., Shi, S., *et al.* (2022) Development of a Novel Biomimetic Mechanical Hand Based on Physical Characteristics of Apples. *Agriculture*, **12**, Article 1871. https://doi.org/10.3390/agriculture12111871

[14] Avigad, G., Salomon, S., Kahani, A. and Koster, Y. (2022) Robotic Fruit Harvesting Machine with Fruit-Pair Picking and Hybrid Motorized-Pneumatic Robot Arms. US Patent No. 11477942.

[15] Silwal, A., Davidson, J.R., Karkee, M., Mo, C., Zhang, Q. and Lewis, K. (2017) Design, Integration, and Field Evaluation of a Robotic Apple Harvester. *Journal of Field Robotics*, **34**, 1140-1159. https://doi.org/10.1002/rob.21715

[16] Zhou, K., Xia, L., Liu, J., Qian, M. and Pi, J. (2022) Design of a Flexible End-Effector Based on Characteristics of Tomatoes. *International Journal of Agricultural and Biological Engineering*, **15**, 13-24. https://doi.org/10.25165/j.ijabe.20221502.6672

[17] Wang, Z., Zou, L., Su, X., Luo, G., Li, R. and Huang, Y. (2021) Hybrid Force/Position Control in Workspace of Robotic Manipulator in Uncertain Environments Based on Adaptive Fuzzy Control. *Robotics and Autonomous Systems*, **145**, Article ID: 103870. https://doi.org/10.1016/j.robot.2021.103870

[18] Zhang, H., Li, L., Zhao, J. and Zhao, J. (2021) The Hybrid Force/Position Anti-Disturbance Control Strategy for Robot Abrasive Belt Grinding of Aviation Blade Base on Fuzzy PID Control. *The International Journal of Advanced Manufacturing Technology*, **114**, 3645-3656. https://doi.org/10.1007/s00170-021-07122-2